Journal of Catalysis **192,** 236–247 (2000)
doi:10.1006/jcat.2000.2837, available online at http://www.idealibrary.com on IDEAL®

Fe/ZSM-5 Prepared by Sublimation of $FeCl_3$: The Structure of the Fe Species as Determined by IR, ^{27}Al MAS NMR, and EXAFS Spectroscopy

Pasqualino Marturano, Lucie Drozdová, Andreas Kogelbauer,[1] and Roel Prins[2]

Laboratory for Technical Chemistry, Swiss Federal Institute of Technology (ETH), ETH-Zentrum, Universitätstrasse 6, Zürich, CH-8092 Switzerland

Received December 8, 1999; revised January 25, 2000; accepted January 27, 2000

The state of the iron in two different Fe/ZSM-5 samples prepared by sublimation of $FeCl_3$ was investigated by EXAFS, IR, ^{27}Al MAS NMR, XRD, and nitrogen adsorption measurements. In one Fe/ZSM-5 (Fe/Al = 1) sample, EXAFS revealed for the first time the presence of diferric (hydr)oxo-bridged binuclear clusters, whose structures differ from those postulated in the literature, resembling that of the methane monooxygenase enzyme. IR showed that binuclear Fe complexes are located at the ion-exchange positions of the zeolite, compensating one or two lattice charges. The remainder of the charge-compensating sites are Brønsted hydroxyls. On both zeolites, the NMR detection of the framework Al atoms (54 ppm) is strongly perturbed by the paramagnetic effects induced by the Fe ions. The intensity of this peak parallels that of the Brønsted hydroxyls in the IR spectra, thus reflecting the presence of Fe species at ion-exchange positions. In a second Fe/ZSM-5 (Fe/Al = 0.8) sample, the iron was present predominantly in the form of large hematite particles (EXAFS, XRD), although a minor fraction of binuclear species might be present as well. The formation of different species seems to be related to different hydrolysis processes occurring on the two zeolites upon washing of the preparation after the sublimation of $FeCl_3$. It is also suggested that the final state of the Fe depends on the presence of extraframework Al species as well as the crystallite size of the zeolite used.

Key Words: **Fe/ZSM-5; deNOx; sublimation; Fe *K*-edge; EXAFS; oxo-bridged species; monooxygenase; contact interactions.**

INTRODUCTION

Owing to their redox properties, iron-exchanged zeolites have been known and investigated for many years (1–3). Recently these catalysts have attracted renewed attention as it has been shown that Fe/ZSM-5 with a high degree of ion exchange (Fe/Al ∼ 1) possesses remarkable properties for the selective catalytic reduction (SCR) of nitrogen oxides (NOx) by hydrocarbons (4). Besides its having a higher activity than Cu/ZSM-5, especially its insensitivity towards the presence of H_2O and SO_2 as well as its exceptional hydrothermal stability make Fe/ZSM-5 stand out among the zeolite-based catalyst systems. As the original preparation method published by Feng and Hall (4) lacked reproducibility (5–8), alternative ion-exchange procedures have been investigated including sublimation of $FeCl_3$ under exclusion of air (5), solid-state ion exchange (9), and aqueous ion exchange using different types of Fe-salt solutions (8, 10, 11). Among these methods, the sublimation of $FeCl_3$ turned out to be the best route to attain a high degree of ion exchange and simultaneously limit the formation of iron oxide, which is inactive in the SCR of NOx (9).

Joyner and Stockenhuber have recently shown that the nature of the Fe species in Fe/ZSM-5 zeolites depends markedly on the ion-exchange method used for the preparation as well as the type of pretreatment of the catalysts (10). On the basis of EXAFS results, these authors concluded that in Fe/ZSM-5 zeolites prepared using different ion-exchange methods (i.e., conventional aqueous ion exchange, solid-state ion exchange, and ion exchange in methanolic solution) Fe was stabilised in different forms ranging from isolated metal ions to large oxide clusters and oxygen-containing nanoclusters. These latter species, which were particularly stable under reductive conditions (H_2, 1100 K), were concluded to have an average composition of Fe_4O_4 and a structure similar to those of ferredoxin (Fe_3S_4) or high-potential iron protein (HIPIP).

Although little is known about the nature of the active species in Fe/ZSM-5 prepared by sublimation of $FeCl_3$, the results reported in the literature indicate that also in this case the final form of the Fe depends at least on the type of activation treatments of the zeolite, its Si/Al ratio, and the iron loading. A model for the active species has been proposed by Sachtler and co-workers (5, 12, 13). On the basis of FTIR, TPR, and ESR data, it was concluded that after sublimation most Fe species are present as isolated species

[1] Present address: Department of Chemical Engineering and Chemical Technology, Imperial College of Science, Technology and Medicine, London SW7 2BY, United Kingdom.

[2] To whom correspondence should be addressed. Fax: +41-1-632 1162. E-mail: prins@tech.chem.ethz.ch.

0021-9517/00 $35.00

in tetrahedral coordination, which upon subsequent hydrolysis and calcination in O_2 at 823 K are transformed into oxo-bridged binuclear ($[(HO)–Fe–O–Fe–(OH)]^{2+}$) complexes compensating two negative charges of the lattice (13). These complexes, which can undergo reversible reduction in hydrogen at 773 K, account for about 85% of the total Fe content. The remainder of the iron was transformed into Fe_2O_3 upon hydrolysis and calcination. Kucherov *et al.* (7) reported ESR results for Fe/ZSM-5 (Si/Al = 15) prepared by sublimation of $FeCl_3$ that were very similar to those shown in (13). However, in their case a reductive treatment under hydrogen at 673 K led to the irreversible formation of an agglomerated ferromagnetic species. Ma and Grünert, using a somewhat modified sublimation technique consisting of the sublimation of $FeCl_3$ *in vacuo* followed by calcination in air without any intermediate hydrolysis step, obtained an Fe/ZSM-5 (Si/Al = 14) catalyst that was highly active in the SCR of NOx with ammonia (14). Their catalyst, however, exhibited much lower activity in the SCR with *i*-butane compared to the one reported in the original work by Feng and Hall (4), thus suggesting that different sites might be active for the two reactions. Finally, Lobree *et al.* have shown that the oxidation state of the Fe depends also on the Fe content of the zeolite (15). Iron was found as Fe^{III} for ratios of Fe/Al < 0.56, whereas above this level the formation of iron oxide as well as Fe^{II} (formed via autoreduction of the $Fe^{3+}(OH^-)_2$ species accompanied by the release of molecular oxygen and water) occurred. In this investigation, however, Fe/ZSM-5 was prepared by solid-state ion-exchange with $FeCl_3$ under vacuum followed by washing of the zeolite.

In this work we present the results of the characterisation (EXAFS, FTIR, ^{27}Al NMR, XRD, N_2 adsorption) of two Fe/ZSM-5 zeolites prepared using the sublimation method reported in (5). Although the parent H/ZSM-5 zeolites had a similar composition, the ion-exchange resulted in two Fe/ZSM-5 samples with different structural properties. For one of the two Fe/ZSM-5 (Si/Al = 20) samples investigated, EXAFS analysis provided evidence for the formation of a binuclear oxo-bridged species different from that postulated in the literature. In the second Fe/ZSM-5 (Si/Al = 15) sample, iron was found mainly in the form of hematite. FTIR results indicate that the formation of different Fe species on the two zeolites is related to different hydrolysis processes, which took place upon washing of the zeolites after the sublimation. The difference between the two samples was also related to the presence of extraframework Al species and the crystallite size of the zeolite.

EXPERIMENTAL

ZSM-5 samples were provided by Süd-Chemie AG (Na-MFI-46 P, Si/Al = 20) and Zeolyst (CBV 3024G, NH_4 form, Si/Al = 15). The zeolites were calcined at 873 K overnight in static air under shallow-bed conditions prior to use. The proton form of both samples was obtained after ion-exchange with a 1 M aqueous solution of NH_4NO_3 under reflux conditions followed by calcination at 823 K. The ammonium exchange was repeated two times. The Süd-Chemie and Zeolyst zeolites will hereafter be referred to as H/ZSM-5(20) and H/ZSM-5(15), respectively, where the number in parentheses indicates the Si/Al ratio. The iron exchange was carried out by sublimation of $FeCl_3$ under exclusion of air as described in (5). After the exchange the samples were washed with deionised water, dried in air, and subsequently calcined at 873 K in flowing O_2 for 2 h. The iron-exchanged Süd-Chemie and Zeolyst zeolites will hereafter be referred to as Fe/ZSM-5(20) and Fe/ZSM-5(15), respectively. The chemical composition of the zeolites was determined by atomic absorption spectroscopy on a Varian SpectrAA-10 after dissolution in hydrofluoric acid. X-ray powder diffraction patterns of the modified zeolites were recorded from 5° to 60° 2Θ on a Siemens D5000 diffractometer using Cu $K\alpha$ radiation at a step size of 0.02°.

Infrared spectra of self-supporting zeolite wafers were recorded at ambient temperature on a Mattson Galaxy 6020 IR spectrometer equipped with an MCT detector at a resolution of 4 cm^{-1}. Prior to IR measurements samples were outgassed *in situ* at 773 K overnight at a pressure below 10^{-4} Pa. For the comparison of spectra taken on different wafers, spectra were normalised using the intensities of the overtone bands of the T–O–T lattice vibrations at 2000 and 1878 cm^{-1}.

Solid-state MAS NMR measurements were carried out using a Bruker AMX400 spectrometer at a magnetic field of 9.4 T. ^{27}Al MAS NMR spectra were recorded on fully hydrated samples at a resonance frequency of 104.26 MHz. The ^{27}Al chemical shifts were referenced to $Al(H_2O)_6^{3+}$ in a 1 M aqueous solution of $Al(NO_3)_3$. For each spectrum 2160 scans were acquired with a recycling time of 10 s. Rotors were spun at 5 kHz with pulse lengths of 1 μs, corresponding to a flip angle $<\pi/12$. These parameters ascertained quantitative determination of Al species.

Nitrogen adsorption at 77 K was carried out on a Micromeritics ASAP 2000M volumetric analyser. The zeolites were outgassed prior to analysis under vacuum at 673 K for at least 5 h. The specific surface area was evaluated using the BET method, while the micropore surface area was determined according to the *t*-plot method.

EXAFS measurements were carried out at the European Synchrotron Radiation Facility (ESRF) in Grenoble (France) on the Swiss-Norwegian Beam Line (SNBL). The electron energy and ring current were 6 GeV and 130–200 mA, respectively. At SNBL the incident X rays are monochromated by a Si (111) channel-cut monochromator and harmonics are rejected by a gold-coated mirror. Prior to the measurements samples were treated at 673 K (3 K/min) in flowing He for at least 1 h. Fe *K*-edge spectra

were recorded in transmission mode at liquid nitrogen temperature in order to decrease the Debye–Waller factors. Data were analysed by standard procedures using the XAFS data analysis program XDAP Version 2.2.2 (16, 17). The Fourier transformation (FT) of the k^3-weighted EXAFS function was carried out in the range 3.4–13.8 $Å^{-1}$ and the Fourier-filtered data were fitted in *R*-space in the range 1–4 Å. The multiple-shell fitting procedure was used to calculate interatomic distances (*R*), coordination numbers (*CN*), Debye–Waller factors ($\Delta\sigma^2$), and edge energy shifts (ΔE_0). The validity of a fit was checked by the fitting of k^1-, k^2-, and k^3-weighted spectra in *R*-space as well as in *k*-space. The quality of a fit was estimated from the values of the variances of the imaginary (V_{Im}) and absolute (V_{Abs}) parts of the FT and from the value of the goodness of the fit (ε_v^2) (16, 17). The variance represents the residual between the observed and calculated spectra in the fitted range. The ε_v^2 takes the number of free parameters into account and is used to determine whether the addition of new parameters makes sense. Reference spectra were generated with the FEFF7 program (18) using XRD data for Fe_2O_3 and Fe_2SiO_4 (19, 20) as input parameters in order to obtain nonstructural parameters such as scattering amplitudes and phase shifts for individual back-scattering pairs of atoms. An advantage of the FEFF7 program is that it can accurately model multiple scattering as well as single scattering contributions to XAFS. The program ATOMS (21) was employed to calculate coordination numbers and interatomic distances from reported XRD data of reference compounds.

RESULTS

Elemental Analysis (AAS) and X-Ray Diffraction (XRD)

The results of the elemental analyses of the iron-containing zeolites revealed that after sublimation of $FeCl_3$ the Fe loadings were Fe/Al = 1 (3.6 wt% Fe) for Fe/ZSM-5(20) and Fe/Al = 0.8 (4.5 wt% Fe) for Fe/ZSM-5(15). The concentrations of sodium and chlorine were below the detection limits. The XRD powder patterns of the Fe-containing zeolites showed that in both cases the crystallinity was retained after the iron loading. After the treatment in oxygen at 873 K, low-intensity diffraction lines at 33.15 2Θ and 35.65 2Θ were detected on Fe/ZSM-5(15), which indicated the presence of traces of hematite (diffraction patterns not shown). No evidence of any other phase besides ZSM-5 was found on FeZSM-5(20). The colors of the samples after the calcination in oxygen were orange and light brown for Fe/ZSM-5(15) and Fe/ZSM-5(20), respectively.

Nitrogen Adsorption

The two ZSM-5 zeolites used in this study exhibited remarkable differences in their textural properties as shown by the nitrogen adsorption measurements (Table 1). The total N_2 uptake of H/ZSM-5(20) was much higher than that of H/ZSM-5(15) and the total pore volumes estimated were 0.72 and 0.29 cm^3/g, respectively. The micropore volumes were almost the same in both cases, while the external surface area calculated for H/ZSM-5(20) (75 m^2/g) was higher than that for H/ZSM-5(15) (23 m^2/g). Furthermore, the isotherm plots of H/ZSM-5(20) showed a broad capillary condensation at quite high values of nitrogen relative pressure ($P/P_0 = 0.8$), which is not observed on H/ZSM-5(15). These data suggest that H/ZSM-5(20) possesses rather small crystals compared to H/ZSM-5(15), and mesopores are also most probably present. After the Fe loading the two Fe/ZSM-5 samples showed slight differences compared to the respective parent zeolites. The negligible decreases in the micropore volumes suggest that no occlusion of the pores due to the formation of an additional phase occurred on both zeolites.

TABLE 1

Nitrogen Adsorption Results

	Total pore volume (cm^3/g)	Micropore volume (cm^3/g)	External surface area (m^2/g)
H/ZSM-5(20)	0.72	0.17	75
H/ZSM-5(15)	0.29	0.16	23
Fe/ZSM-5(20)[a]	0.67	0.15	70
Fe/ZSM-5(15)[a]	0.26	0.14	20

[a] After sublimation of $FeCl_3$ followed by hydrolysis and treatment in O_2 at 773 K.

FTIR Spectroscopy

In Fig. 1 the IR spectra in the O–H stretching region (3000–3900 cm^{-1}) of Fe/ZSM-5(20) after each step of the preparation are shown. For comparison the spectrum of

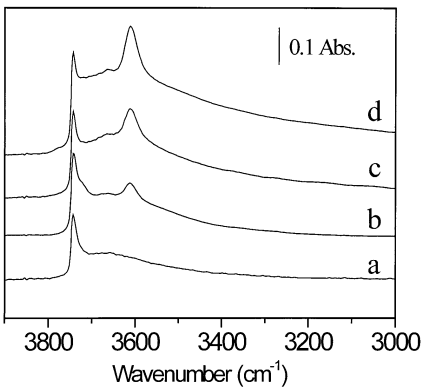

FIG. 1. IR spectra (RT) after outgassing at 773 K of (a) Fe/ZSM-5(20) after sublimation, (b) after sublimation and hydrolysis, (c) after sublimation, hydrolysis, and calcination, and (d) parent H/ZSM-5(20).

the parent zeolite H/ZSM-5(20) is also given. On H/ZSM-5(20) two bands were observed at 3743 and 3610 cm^{-1}, which are assigned to external silanol groups and to bridged Si(OH)Al hydroxyls (Brønsted acid sites) (22, 23). A very weak band was also detected at 3660 cm^{-1} and assigned to hydroxyls groups associated with extraframework Al species (22). The sublimation of $FeCl_3$ caused the complete disappearance of the Brønsted hydroxyls band (3610 cm^{-1}), while the silanol band (3743 cm^{-1}) became less intense (Fig. 1, spectrum a). After washing of the zeolite the intensity of the silanol band was completely restored, whereas the band associated with the Brønsted hydroxyls reappeared but with a much lower intensity. In addition, a new band appeared at 3725 cm^{-1}. After the subsequent calcination in oxygen this shoulder disappeared and, at the same time, the band at 3610 cm^{-1} increased to about 50% of its original intensity as estimated by comparison of the integrated intensity with that of H/ZSM-5(20). The same type of evolution was observed for the band at 3610 cm^{-1} on Fe/ZSM-5(15) (spectra not shown). In this case, after the calcination the intensity of the band reached only 30% of that observed for the parent H/ZSM-5(15). The recovered intensity of the 3610 cm^{-1} band is in good agreement with the reports in the literature (5, 13, 24) and indicates that variable amounts of the Fe species at ion-exchange positions are displaced by protons during the treatments following the sublimation. As for the shoulder at 3725 cm^{-1} on Fe/ZSM-5(20), we tentatively assign it to the stretching vibration of OH groups associated with hydrolysed Fe species formed upon washing of the zeolite. This assignment is supported by the observation of surface OH groups with very similar frequencies on some iron oxides such as hematite, akaganéite, and maghemite (25).

The spectra of Fe/ZSM-5(20) together with that of the parent H/ZSM-5(20) in the frequency range 1200–2200 cm^{-1} are depicted in Fig. 2. On H/ZSM-5(20) (Fig. 2, spectrum d) four bands were detected at 2000, 1878, 1642, and 1470 cm^{-1}, which were assigned to overtones and combination framework modes (22). After the sublimation of $FeCl_3$ and the *in situ* outgassing at 773 K, Fe/ZSM-5(20) showed a spectrum very similar to that of the parent zeolite (Fig. 2, spectrum a), the only difference being two very weak bands at 1536 and 1461 cm^{-1}. More remarkable changes were induced by the subsequent hydrolysis step. New bands, which evolved upon increasing the evacuation temperature from RT to 773 K, were detected in the frequency range 1700–1300 cm^{-1}. The spectrum obtained after outgassing overnight at 773 K exhibited bands at 1554, 1456, and 1421 cm^{-1} accompanied by weak shoulders at 1666, 1569, and 1353 cm^{-1} (Fig. 2, spectrum b). These bands disappeared upon treatment of the sample in O_2 at 773 K (Fig. 2, spectrum c). By comparison of these spectra with those reported in the literature for iron oxides (25) and $FeCl_3$ (26), it can be excluded that these bands correspond to the deformation modes of hydroxylated Fe species or to Fe–Cl modes. In both cases, the IR radiation is absorbed in rather different frequency ranges. Nevertheless, although these bands cannot be precisely assigned, it is important to notice that the spectroscopic features in the range 1700–1300 cm^{-1} were peculiar for the Fe/ZSM-5(20) zeolite and were not observed on Fe/ZSM-5(15) (inset Fig. 2). This finding suggests that hydrolysis may give rise to different types of species on different Fe-loaded zeolites.

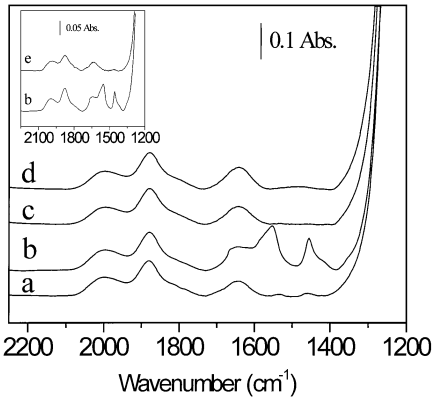

FIG. 2. IR spectra (RT) after outgassing at 773 K of (a) Fe/ZSM-5(20) after sublimation, (b) after sublimation and hydrolysis, (c) after sublimation, hydrolysis, and calcination, (d) parent H/ZSM-5(20), and (e) Fe/ZSM-5(15) after sublimation and hydrolysis (inset).

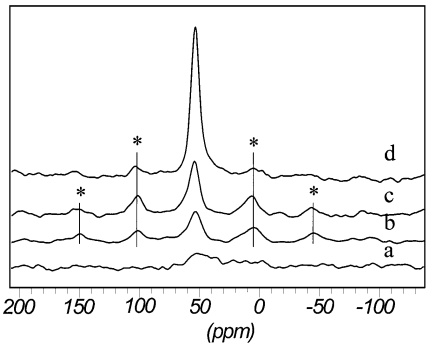

FIG. 3. ^{27}Al MAS NMR spectra of (a) Fe/ZSM-5(20) after sublimation, (b) after sublimation and hydrolysis, (c) after sublimation, hydrolysis, and calcination, and (d) parent H/ZSM-5(20).

^{27}Al MAS NMR

^{27}Al MAS NMR spectroscopy was carried out on Fe/ZSM-5(20) and Fe/ZSM-5(15) after each step of the preparation. The spectra are reported in Figs. 3 and 4 together with those of the H/ZSM-5 zeolites used as starting materials. For both H/ZSM-5 zeolites a resonance was detected at about 54 ppm (Figs. 3 and 4, spectra d), which is assigned to tetrahedrally coordinated Al atoms in lattice positions. The two weak signals on Fe/ZSM-5(20) at 5 and 105 ppm (Fe/ZSM-5(15), −40 and 155 ppm) are spinning

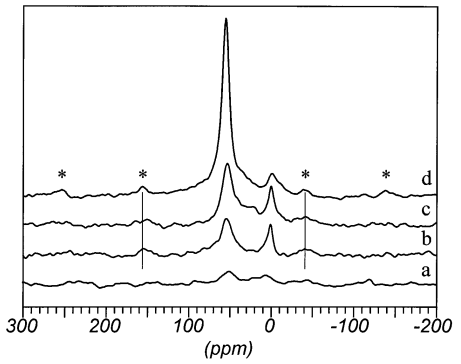

FIG. 4. ^{27}Al MAS NMR spectra of (a) Fe/ZSM-5(15) after sublimation, (b) after sublimation and hydrolysis, (c) after sublimation, hydrolysis, and calcination, and (d) parent H/ZSM-5(15).

side bands due to the quadrupolar interactions of ^{27}Al nuclei. On H/ZSM-5(15) an additional resonance was detected at 0 ppm (Fig. 4, spectrum d), which is assigned to Al in octahedral coordination, namely extraframework Al species. After the sublimation of $FeCl_3$, the intensity of the 54 ppm line was dramatically reduced and only a very weak signal was detected on both Fe/ZSM-5 samples (Figs. 3 and 4, spectra a). This marked suppression is a direct consequence of the paramagnetism of the Fe ions, whose unpaired electrons generate a local magnetic field that strongly perturbs the resonance of the ^{27}Al nuclei (27, 28). Paramagnetic effects were also observed on the peak at 0 ppm in the spectrum of Fe/ZSM-5(15) (Fig. 4, spectrum a). The intensity of this peak, however, was fully restored and even slightly increased after the hydrolysis and calcination, thus suggesting that dealumination of the zeolite might have occurred (Fig. 4, spectra b and c).

The hydrolysis and calcination treatment caused the intensity of the signal at 54 ppm to increase on both Fe/ZSM-5 samples. This recovery of the signal intensity paralleled that observed for the Brønsted acid sites band (3610 cm^{-1}) in the corresponding IR spectra and therefore confirms the displacement of the iron species from ion-exchange positions.

EXAFS

Experimental and Fourier-filtered k^3-weighted EXAFS χ functions of the samples after calcination are shown in Fig. 5. By comparing the χ functions, it becomes evident that the spectra of the Fe_2O_3 (Fig. 5a) and Fe/ZSM-5(15) (Fig. 5b) samples are similar, while the spectrum of Fe/ZSM-5(20) (Fig. 5c) is significantly different. The EXAFS results obtained from the fitting of the Fe_2O_3 spectrum were compared with coordination numbers and interatomic distances calculated using reported XRD data (19) and good agreement was observed (see Table 2), as expected. The fitted Fe_2O_3 spectrum in reciprocal space is shown in Fig. 5a and the Fourier transformations of the Fourier-filtered experimental data and of the fitted spectrum are presented in Fig. 6. In view of the similarity between the χ functions, the EXAFS results for Fe_2O_3 were used as input parameters for fitting the spectrum of the Fe/ZSM-5(15) sample. The fitted spectrum in reciprocal space is presented in Fig. 5b and FTs of the filtered and fitted spectra are shown in Fig. 7. It can be seen that the five-shell model used to fit the spectrum of Fe_2O_3 is sufficiently good also for the Fe/ZSM-5(15) sample (Fig. 7). Consequently, the presence of Fe_2O_3 clusters was confirmed. This result is in good agreement with the above-mentioned XRD results. From a close examination of the fit of Fe/ZSM-5(15) it can be seen that the five-shell fit is not as good as that obtained for Fe_2O_3 in the range from 1 to 2.4 Å (phase-uncorrected FT), the range characteristic of Fe–O shells. The results suggest slight differences in the coordination numbers in comparison with the results

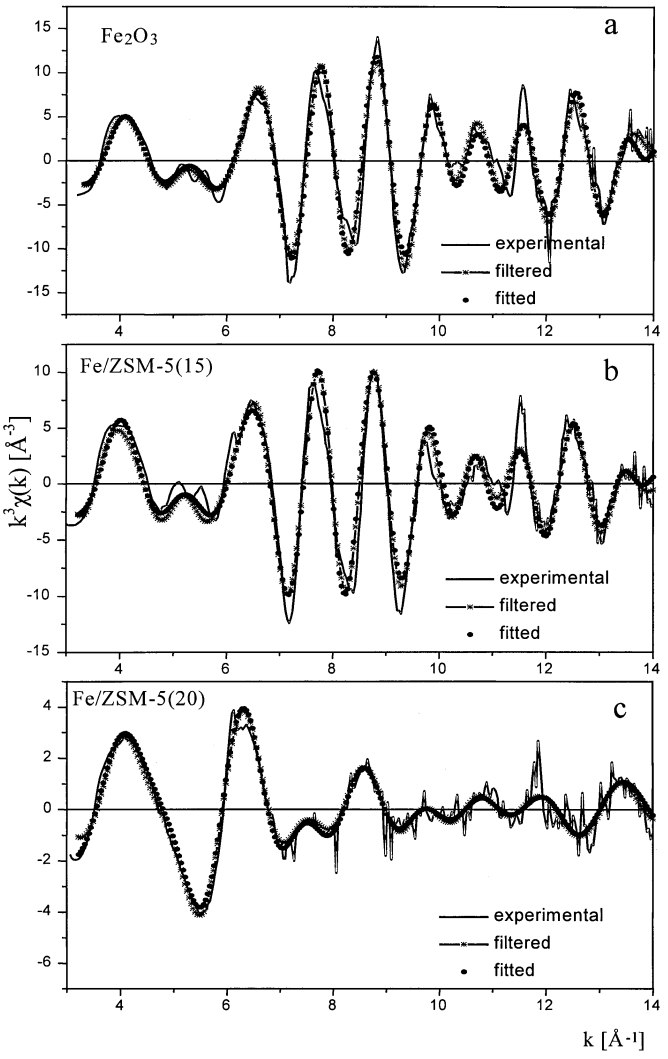

FIG. 5. Experimental, Fourier-filtered, and fitted EXAFS χ functions of (a) Fe_2O_3, (b) Fe/ZSM-5(15), and (c) Fe/ZSM-5(20) (model D) zeolites.

TABLE 2

EXAFS Results

	R (Å)	CN	$\Delta\sigma$ (10^{-3} Å^2)	ΔE_0 (eV)
		Fe_2O_3		
1 Fe–O	1.94, 1.95[a]	3.0, 3.0[a]	0.1	−1.8[b]
2 Fe–O	2.06, 2.11[a]	3.0, 3.0[a]	2.1	9.2[b]
3 Fe–Fe	2.95, 2.97[a]	3.0, 3.0[a]	0.8	−0.6[b]
4 Fe–Fe	3.39, 3.36[a]	2.2, 3.0[a]	3.6	−6.9[b]
5 Fe–O	3.73, 3.79[a]	3.1, 3.0[a]	8.2	−12.2[b]
		ε_v^{2c} 0.14		
		V_{Im}[d] 0.54		
		V_{Abs}[d] 0.21		
		Fe/ZSM-5(15)		
1 Fe–O	1.96	3.6	1.7	1.7[b]
2 Fe–O	2.11	2.4	0.0	5.7[b]
3 Fe–Fe	2.95	3.5	1.1	3.5[b]
4 Fe–Fe	3.40	3.0	0.9	−6.5[b]
5 Fe–O	3.74	3.9	5.9	−12.3[b]
		ε_v^2 0.42		
		V_{Im} 0.34		
		V_{Abs} 0.21		
		Fe/ZSM-5(20), Model C		
1 Fe–O	1.82	0.5	4.8	−6.9
2 Fe–O	1.94	3.6	3.0	8.7
3 Fe–Fe	2.53	0.6	8.5	3.2
4 Fe–Fe	3.06	0.7	2.1	−2.5
		ε_v^2 0.12		
		V_{Im} 0.32		
		V_{Abs} 0.15		
		Fe/ZSM-5(20), Model D		
1 Fe–O	1.83	1.2	2.4	−7.1
2 Fe–O	1.94	4.7	2.5	11.6
3 Fe–O	2.48	1.0	0.7	8.2
4 Fe–Fe	3.05	0.9	4.0	−1.3
		ε_v^2 0.05		
		V_{Im} 0.10		
		V_{Abs} 0.07		

[a] XRD data.
[b] Fixed parameters.
[c] ε_v^2 is the goodness of the fit.
[d] V_{Im} and V_{Abs} are the variances of the imaginary and absolute parts of the FT, respectively. The errors in the fitted parameters are estimated to be $CN \pm 10\%$, $R \pm 0.02$ Å, $\Delta\sigma^2 \pm 10\%$, and $\Delta E_0 \pm 10\%$.

obtained for Fe_2O_3 (Table 2). Since coordination numbers represent averaged values, this points to the possible coexistence of another type of Fe species in addition to the Fe_2O_3 clusters.

The χ function of the Fe/ZSM-5(20) sample is qualitatively different from the χ functions of the Fe/ZSM-5(15) and Fe_2O_3 samples. This difference is reflected in the FTs where two overlapping bands in the range 1–2 Å (uncorrected FT), corresponding to oxygen back-scatterers, are dominant (Fig. 8) in the case of the Fe/ZSM-5(20) sample. This is in contrast to the Fe/ZSM-5(15) (Fig. 7) and Fe_2O_3 (Fig. 6) samples where the two dominant bands are in the

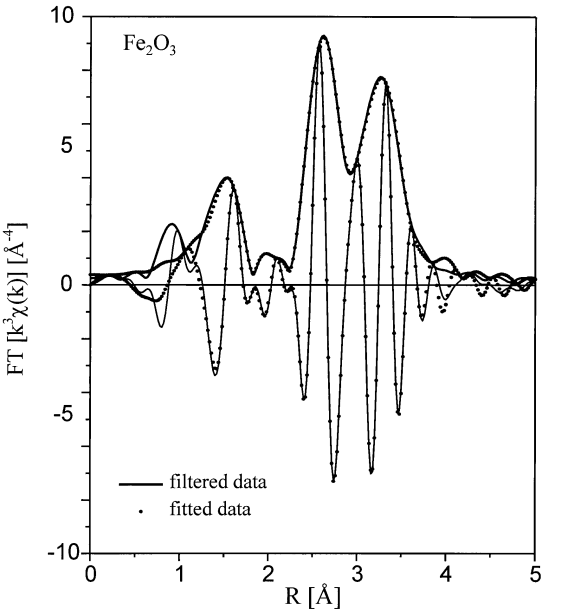

FIG. 6. FT of Fourier-filtered experimental data and fitted data of Fe_2O_3. The wiggling line corresponds to the imaginary part of the χ function.

range 2.0–3.8 Å, which is usually characteristic for contributions from Fe–Fe shells. Various shell models consisting of different possible back-scattering pairs were tried to fit the Fe/ZSM-5(20) spectrum (Table 3). The first two bands in the FT were easily assigned to Fe–O(1) and Fe–O(2)

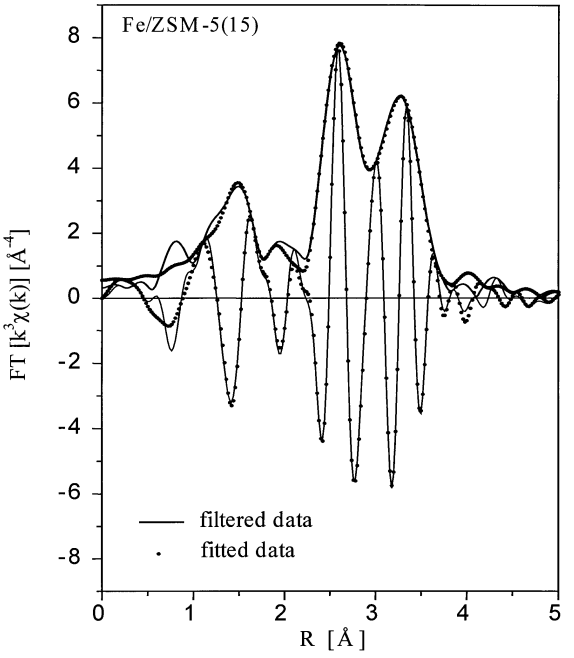

FIG. 7. FT of Fourier-filtered experimental data and fitted data of Fe/ZSM-5(15). The wiggling line corresponds to the imaginary part of the χ function.

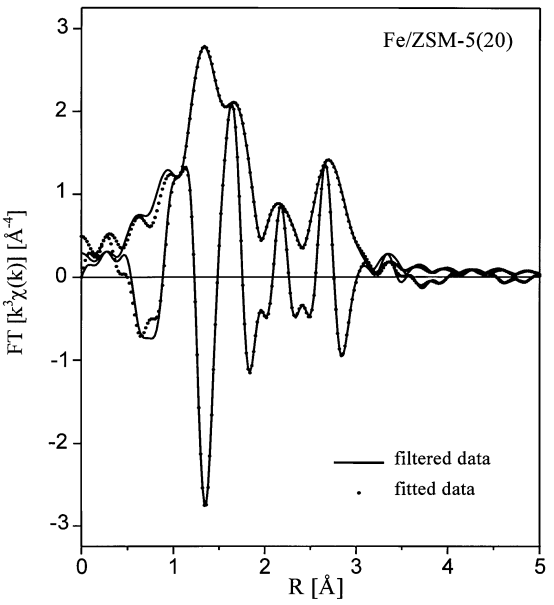

FIG. 8. FT of Fourier-filtered experimental data and fitted data of Fe/ZSM-5(20) using model D. The wiggling line corresponds to the imaginary part of the χ function.

shells, and so these two oxygen shells were included in all the models tried. The assignment of third and fourth shells was more difficult and this process is described in the Discussion. The best results were obtained with model D, when the goodness of the fit in *R*- as well as in *k*-space was considered. Also, reasonable values of Debye–Waller factors and edge energy shifts, and fitting using k^1-, k^2-, as well as k^3-weighted spectra, helped us to choose the most probable model. The best fit of the Fe/ZSM-5(20) spectrum using model D is shown in reciprocal space in Fig. 5c and the FT is presented in Fig. 8. The results of the fitting are summarised in Table 2 and point to the presence of some new small iron oxide clusters consisting of only two iron atoms. The presence of large Fe_2O_3 clusters can be excluded, in agreement with the XRD results.

TABLE 3

EXAFS Shell Models Used for Fitting

	Fe Shells			
	1 + 2	3	4	Fe species
Model A	O	Si/Al		Fe incorporated into framework,
	O	Si/Al	Si/Al	Fe ions (monoatomic) at
	O	O	Si/Al	ion-exchange positions
Model B	O	Fe	Si/Al	Clusters like Fe_4O_4 (10)
Model C	O	Fe	Fe	Fe binuclear species or clusters like
	O	Si/Al	Fe	Fe_4O_4
Model D	O	O	Fe	Fe binuclear species

DISCUSSION

The results obtained in this work confirm that Fe/ZSM-5 with a high degree of ion exchange can easily be prepared by sublimation of $FeCl_3$. The nature of the iron species hosted in the zeolite, however, depends on the characteristics of the ZSM-5 used. As clearly shown by the EXAFS results, Fe species with different structures were formed on the two Fe/ZSM-5 zeolites prepared following exactly the same procedure. In this section we will discuss the different structures observed and the possible reasons for these differences.

On both H/ZSM-5 zeolites the sublimation of $FeCl_3$ resulted in the complete replacement of the protons at ion-exchange positions by Fe species, as indicated by the disappearance of the 3610 cm^{-1} band in the IR spectra (Fig. 1) and the iron concentration in the zeolites (Fe/Al = 1). The fact that the elemental analysis indicated a ratio of Fe/Al = 0.8 for Fe/ZSM-5(15) can be explained by the presence of extraframework Al species (Fig. 4), which do not have Brønsted acid sites associated that can be exchanged.

The paramagnetic effects observed on the ^{27}Al MAS NMR spectra of the Fe zeolites (Figs. 3 and 4) confirm the effective location of Fe species at ion-exchange positions concluded from the IR results. The presence of paramagnetic species as charge-compensating species causes a shortening of the nuclear relaxation time of the framework Al atoms, which results in an apparent loss of intensity of the peak at 54 ppm owing to line broadening. The paramagnetism of the Fe ions also brought about a more intense and extended side band pattern of the NMR spectra. This perturbation of the spectrum arises from the anisotropic dipolar interaction between the electron spin of the Fe ions and the nuclear spin of the Al ions (pseudocontact interactions).

After the sublimation, some Fe cations react with the Al–OH groups of the extraframework Al particles causing the distortion of the peak at 0 ppm (Fig. 4, spectrum a), which, however, became visible again after the hydrolysis and calcination (Fig. 4, spectra b and c). The unchanged intensity of the 0 ppm peak after the hydrolysis and calcination indicates that no paramagnetic interactions occur between Fe and extraframework Al atoms, reflecting therefore a rearrangement of the Fe species inside the zeolite after these treatments. This result is consistent with the fact that extraframework Al species do not bear strong acidic protons and therefore weak interactions (if any) are expected between Fe and these Al species.

The increase in intensity of the peak at 54 ppm (framework Al atoms) and the absence of any peak at 0 ppm (extraframework Al species) on Fe/ZSM-5(20) after hydrolysis and oxidation rules out the possibility that the suppression of the 54 ppm signal is caused by the dislodgement of Al atoms from the lattice by Fe ions. Additionally, from the weak intensity of the spinning side bands observed on the Fe-exchanged zeolites it is excluded that such suppression is due to the incorporation of the Fe ions into the lattice.

As reported in the literature, the ^{27}Al MAS NMR spectra of zeolites containing paramagnetic transition metal ions in the framework exhibit much more intense spinning side bands, which also extend to higher/lower frequencies (29, 30). These findings confirm that the Fe species introduced into the zeolite by the sublimation of $FeCl_3$ are located in extraframework positions within the zeolite pores as previously reported (13). Nevertheless, the introduction into the lattice of a minor fraction of the Fe species cannot be completely ruled out. The reduced intensity of the silanol band in the IR spectrum after the sublimation suggests that some iron species interact with the lattice defects and therefore might have been introduced in the zeolite matrix as concluded for Fe/ZSM-5 with high silica content (13). These iron species, however, were easily removed by washing the zeolite with water as indicated by the increase in intensity of the band at 3743 cm^{-1} due to the silanol groups (Fig. 1, spectrum b).

The hydrolysis and calcination treatments following the sublimation of $FeCl_3$ have been suggested to be the key steps in the formation of the active species in Fe/ZSM-5 zeolites (13). Our results, besides substantiating this hypothesis, also indicate that the final state of Fe may differ according to the characteristics of the zeolite used (e.g., extraframework Al species and crystallite size).

IR spectroscopy showed that upon hydrolysis on both ZSM-5 samples part of the Fe present at the ion-exchange sites was back-exchanged by protons forming Brønsted hydroxyls, whose concentration further increased after the calcination in oxygen. In this respect, it is worth noticing that a parallel increase of the intensity of the framework Al peak (54 ppm) in the ^{27}Al NMR spectra occurred after hydrolysis and calcination. This result, in conjunction with the IR, indicates that the removal of the Fe species from the ion-exchange positions resulted in a decrease of the paramagnetic effects sensed by the Al atoms of the lattice. Since the pseudocontact effects are delocalised anistropic interactions (through-space electron–nucleus dipolar interactions) the rearrangement of the iron species does not seem to completely account for the increase of the Al signal. The concentration of the iron ions in the zeolite, in fact, did not change upon hydrolysis and calcination (AAS) and therefore a lower diminution of the paramagnetic perturbation would be expected for the zeolites after these treatments. It cannot be excluded, therefore, that the prompt recovery of the Al signal might be due also to more localised paramagnetic interactions between the Fe and the Al species (i.e., Fermi contact interactions which are isotropic and act through chemical bonds). This type of interaction has already been reported in the case of aluminosilicate sodalites containing paramagnetic Na_4^{3+} clusters (31, 32). Fermi contact interactions can result in large shifts of the NMR peak even out of the observed spectral range. The NMR spectra presented here did not show any resonance line in the chemical shift range explored that can be attributed to this type of interactions, thereby making such a hypothesis less probable. Further experiments are in progress to ascertain the exact nature of these paramagnetic interactions.

Despite the similar IR and NMR data, EXAFS spectroscopy showed rather different results for the two zeolites. Analysis of the EXAFS spectra demonstrated the presence of Fe_2O_3 clusters in the Fe/ZSM-5(15) sample, in agreement with the XRD measurements. Moreover, EXAFS detected other Fe species, whose exact structure was difficult to determine due to the predominant signal from the hematite phase. These species might possess a structure similar to that of the diferric binuclear clusters determined in Fe/ZSM-5(20) (see below). The presence of hematite as the predominant form of iron in Fe/ZSM-5(15) seems to be in contrast with the IR results. The detection of the oxide phase by XRD and the negligible decrease of the micropore volume after calcination indicate that the Fe oxide is located mainly on the outer surface of the zeolite crystals. Therefore, most of the ion-exchange positions are expected to be occupied by protons, whereas IR showed that only 30% of them were Brønsted acid sites. A possible explanation for this discrepancy could be the presence of positively charged oxide particles that act as charge-balancing ions, as already proposed for extraframework Al species (33). In addition, the negative charge of the zeolite lattice is also compensated by the above-mentioned binuclear species.

The EXAFS results for Fe/ZSM-5(20) were remarkably different from those obtained for Fe/ZSM-5(15) and the evaluation of the EXAFS spectrum is more complicated. EXAFS studies of Fe silicalites successfully confirmed the substitution of Si by Fe ions in the framework of the ZSM-5 structure (34–39). Therefore, an EXAFS model (see Table 3) consisting of only Fe–O and Fe–Si/Al shells was chosen to check the possibility of Fe incorporation into the zeolite framework. The same model can also describe the presence of mononuclear Fe ions exchanged into cationic exchange positions, because also in that case, only Fe–O and Fe–Si/Al shells are expected. As the fitting with model A did not provide a satisfactory fit with the Fe/ZSM-5(20) spectrum, the substitution of Si by Fe ions as well as the location of separate mononuclear Fe ions in cation-exchange positions can be excluded in agreement with the NMR results.

The EXAFS study of Fe/ZSM-5 zeolites prepared using different ion-exchange methods (10) showed the formation of different Fe species, depending on the type of preparation and pretreatment of the catalysts. In particular, on Fe/ZSM-5 prepared by aqueous ion exchange followed by heat treatment in an inert atmosphere, EXAFS analysis revealed the presence of small oxygen-containing nanoclusters assigned to Fe_4O_3 or Fe_4O_4 clusters with a structure similar either to iron–sulphur compounds like ferredoxins (40) or the cubanes of high-potential iron protein (HIPIP) (41). The authors observed the shortening of the Fe–Fe distance from a typical value of 3.00 Å to a very unusual 2.53 Å

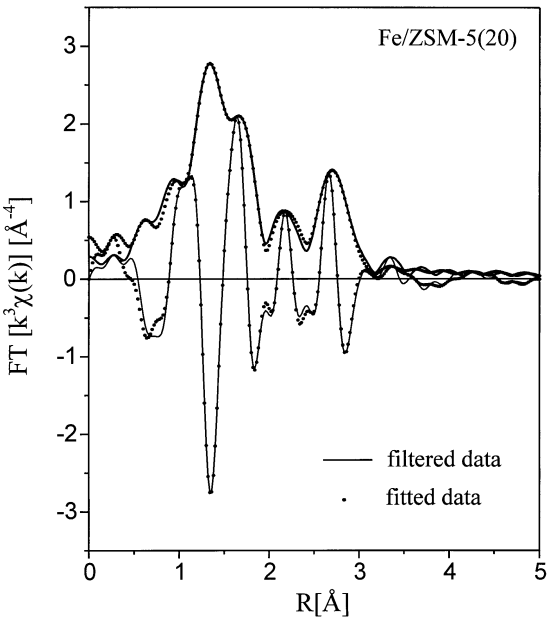

FIG. 9. FT of Fourier-filtered experimental data and fitted data of Fe/ZSM-5(20) using model C. The wiggling line corresponds to the imaginary part of the χ function.

after activation. They compared this value to the distance of 2.67 Å observed in reduced ferredoxins (40). On the basis of these results, we tried to fit the spectrum of Fe/ZSM-5(20) with model B, in which the third and fourth shells are attributed to Fe and Si/Al back-scatterers, respectively. Model B did not yield a good fit either, however. If Fe_4O_4 clusters were present, additional Fe–Fe distances besides the short one at about 2.75 Å should appear, as was observed for various cubane-type Fe_4S_4 clusters (42, 43). We therefore tried a third model, model C, in which it was assumed that the third shell consisted of Fe or Si/Al atoms and the fourth shell of Fe atoms. In contrast to the results of Joyner and Stockenhuber, a fourth shell appeared at a distance of 3.06 Å, typical for Fe–Fe, in addition to a short Fe–Fe distance of 2.53 Å. While this fit looks reasonably good (see Fig. 9), the coordination numbers of the Fe–Fe shells are too low to belong to a Fe_4O_4 cluster (Table 2). This makes it difficult to believe that such clusters are formed. Furthermore, iron–oxygen cubane-type clusters with interatomic distances in the range 2.53–2.75 Å are not known.

Although model C cannot describe the results, it does point to the presence of an Fe–Fe shell around 3.06 Å. The low coordination number suggest that probably only two Fe atoms per cluster are present. This made us consider binuclear Fe clusters, whose existence has already been suggested in the literature (5, 6, 12, 13), as models to explain the EXAFS data. The existence of such a binuclear complex was predicted mainly on the basis of TPR, FTIR, and ESR measurements which gave evidence for separate octahedral binuclear Fe^{3+}–O–Fe^{3+} ions in cationic positions in the zeolite. In a series of studies on the oxidation of methane and benzene on Fe/ZSM-5, Panov and co-workers compared the structure of the active iron sites in ZSM-5 to binuclear active centres in methane monooxygenase (44, 45). The enzyme methane monooxygenase (MMO), found in methanotropic bacteria, catalyses the hydroxylation of methane to methanol, and one of its three protein components, called hydroxylase (MMOH), contains binuclear iron clusters as active centres (46). The first EXAFS study on MMOH showed an average Fe–ligand distance of 1.92 Å and an Fe–Fe distance of 3.05 Å (47). A detailed XAFS analysis of MMOH from *Methylosinus trichosporium* OB3b (48) suggested the presence of two Fe–Fe distances of about 3.0 and 3.4 Å reflecting the population of MMOH molecules with two and one μ-hydroxo bridges in a diiron(III) core structure, respectively (Fig. 10a). This shortening of the Fe–Fe distance from 3.4 to 3.1 Å due

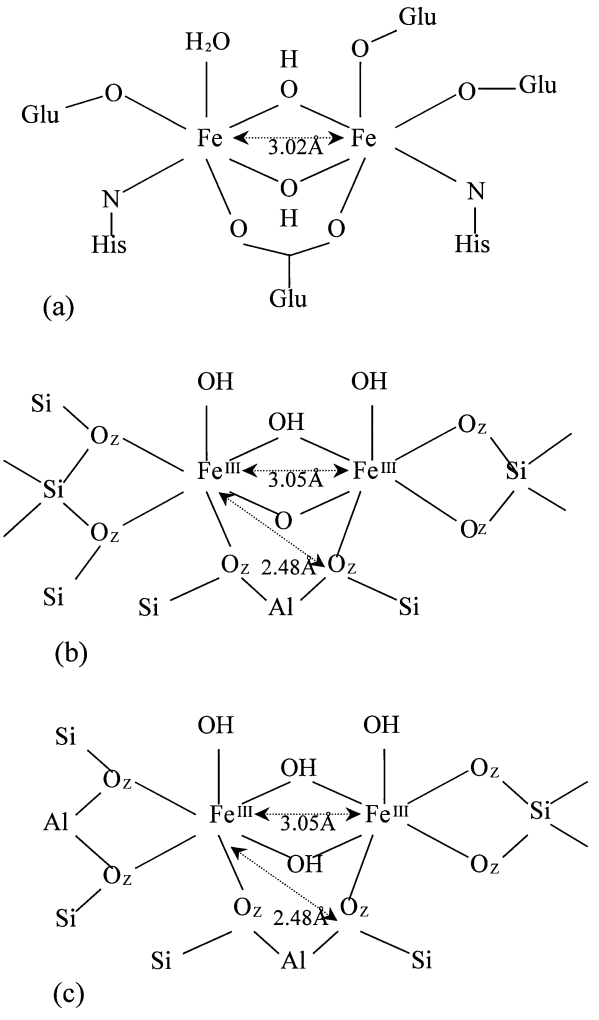

FIG. 10. (a) Structure of MMOH active centre as reported in (48), and proposed Fe_2O_2-type clusters present in the Fe/ZSM-5(20) zeolite compensating (b) one or (c) two lattice charges.

TABLE 4

Summary of Core Structures of Octahedral Diiron Complexes and MMOH

Diamond core	Fe–Fe (Å)	Fe–(μ-O) (Å)	Fe–(μ-OH) (Å)	Ref.
$Fe_2^{III}(\mu\text{-}O)_2$	2.71	1.88		(50)
	2.714	1.841, 1.917		
$Fe_2^{III}(\mu\text{-}O)(\mu\text{-}OH)$	2.83	1.85	1.98	(51)
	2.91	1.82	1.99	(52)
$Fe_2^{III}(\mu\text{-}OH)_2$	3.08–3.16		1.96–2.02	(53–55)
$Fe^{II}Fe^{III}(\mu\text{-}OH)_3$	2.51		1.94	(52)
MMOH (OB3b)	3.02		1.96	(48)
MMOH (Bath)	3.04		1.78, 1.94	(49)

to the presence of two hydroxy-bridging ligands instead of only one hydroxo bridge was observed for the first time in MMO hydroxylase from *Methylococcus capsulatus* (Bath) and it was concluded that the active centre adopts an Fe_2O_2 "diamond core" structure (49). A series of synthetic model complexes containing a mixed-valence Fe_2O_2 core was synthesised (50–55). The crystallographically characterised complexes, which have spectroscopic and catalytic properties relevant to those of MMOH, served as models to explain the roles of active centres in MMOH adopting the Fe_2O_2-type core structure (49).

The observed similarity between the k^3-weighted χ spectrum of the Fe/ZSM-5(20) sample and MMOH (48), as well as the very similar results obtained from fitting the spectra using model D (Table 2) and the EXAFS reported for MMOH (43, 44) (Table 4), enables us to compare our Fe clusters to MMOH active centres. The best fit represented by model D gave an Fe–Fe distance of 3.05 Å which is in excellent agreement with the Fe–Fe distance obtained for the $Fe_2^{III}(\mu\text{-}OH)_2$ core (3.08–3.16 Å) (53–55) as well as for MMOH (3.02 Å) (48). Shu *et al.* (48) argued that the presence of an additional carboxylate bridge besides two hydroxyl bridges in MMOH results in a slight shortening of the Fe–Fe distance from 3.1 to 3.02 Å. They noticed that a distance of about 2.4–2.5 Å, usually assigned to carboxylate or water semibridges (49, 56), was absent, but they admitted that the contribution to the EXAFS signal due to the system disorder is not necessarily significant. Our results show the presence of such a long Fe–O distance of 2.48 Å as well, which in our case could be due to an interaction with the zeolite framework. The coexistence of $Fe_2^{III}(\mu\text{-}O)(\mu\text{-}OH)$ core structures cannot be excluded because the observed Fe–Fe distance of 2.91 Å for model complexes is quite close to the observed distance of 3.02 Å, which could be an average distance of two closely overlapping shells in the distance range 2.9–3.1 Å. In addition, the observed short Fe–O distance of 1.83 Å is typical for the above-mentioned oxo bridges. The presence of a core with two oxo bridges (50–52) can be excluded because of the observed very short Fe–Fe distance of 2.71 Å (50) in comparison with our results. So, the presence of two types of diamond cores such as $Fe_2^{III}(\mu\text{-}OH)_2$ and $Fe_2^{III}(\mu\text{-}O)(\mu\text{-}OH)$ is then highly probable. Some of the oxygens at a distance of 1.94 and 1.83 Å, which are typical for hydroxo and oxo bridges, respectively, can also be assigned to Fe–O (zeolite). However, the sum of the Fe–O coordination numbers clearly points to an octahedral structure, in agreement with published ESR results (7, 13, 24). Assuming the presence of clusters with two types of core structures, (i) two hydroxo bridges and (ii) one hydroxo bridge and one oxo bridge, both accompanied by a third and longer –O–Si/Al–O– bridge, then the observed coordination number between 4 and 5 for the second oxygen shell seems to make sense and, thus, a mixture of these types of octahedral Fe binuclear clusters is proposed to be formed after calcination of the Fe/ZSM-5(20) sample (Figs. 10b and 10c).

Model D was evidently the best model with regard to the goodness of the fit. On the other hand, the fit using model C was reasonably good although the fit for the third shell in the range of 1.9–2.3 Å of the uncorrected FT (real distance 2.4–2.55 Å) was not optimal in comparison with model D. In model C, the third shell (2.53 Å) was assigned to the Fe–Fe distance and this distance can, according to model complexes, correspond to the $Fe^{II}Fe^{III}(\mu\text{-}OH)_3$ core structure with a reported distance of 2.51 Å. This result does not seem to be completely impossible because some autoreduction due to the influence of the X rays during the EXAFS experiment can result in such a mixed-valence species. On the other hand, this fraction would be expected to be minor regarding the treatment at high temperature in oxygen. A very similar Fe–Fe distance has been recently observed in the diiron (μ-1,2 peroxodiferric) intermediate that forms in the early steps of ferritin biomineralization (57). Although also in this case the formation of a peroxo bridge between the two Fe atoms cannot be completely ruled out, the instability of this compound makes this possibility unlikely.

Although it is not possible to discriminate among the different types of structures proposed, the binuclear nature of the Fe species in Fe/ZSM-5(20) has been established. To our knowledge, this is the first time that direct experimental evidences unambiguously proved the presence of binuclear Fe clusters in Fe/ZSM-5 zeolite, the existence of which had been postulated on the basis of TPR and ESR investigations (5, 12, 13). The coordination of the Fe ions as deduced by the EXAFS analysis, however, is rather different from that proposed in the literature.

IR results, supported by Al NMR, allow us to conclude that the Fe complexes are located at the ion-exchange positions of the zeolite, bearing an overall monopositive charge. In this form they act as extraframework counterions and compensate half of the negative charges of the lattice. The monopositive charge is most likely determined by the presence of coordinated OH groups, which are formed

during the hydrolysis and calcination. This type of binuclear complex is rather different from that suggested in the literature (5, 12, 13), which features both metal atoms bound at ion-exchange positions. Nevertheless, it reasonably accounts for all the experimental findings obtained on Fe/ZSM-5(20). In particular, it explains why the removal of Fe species from the ion-exchange positions upon calcination is not followed by the formation of an oxidic phase. If iron oxide was formed it would involve 50% of the Fe present and, therefore, the EXAFS spectrum of Fe/ZSM-5(20) should appear as a combination of the spectra of the Fe oxide and the binuclear species. Besides, this type of complex also accounts for the presence of a relatively high concentration of Brønsted acid sites (50%) and the decrease in the paramagnetic effects observed in the ^{27}Al NMR spectra after washing and calcination of the zeolite. A recent density functional study of oxygen-bridged Cu species in Cu/ZSM-5 catalyst strongly supports our interpretation of the EXAFS data. According to these calculations, species like $Cu^{II}_2(\mu$-O) and $Cu^{II}_2(\mu$-$O)_2$ are predicted to have high stability and can be easily accommodated in the zeolite cavities (58).

As for the reasons for the formation of different Fe species on the two ZSM-5 samples investigated, the IR results strongly suggest that it might be related to the hydrolysis process occurring during the washing of the zeolites. The IR spectrum of Fe/ZSM-5(20) after the sublimation and the hydrolysis was, in fact, substantially different from that of Fe/ZSM-5(15) (Fig. 2, inset). The spectrum of the former zeolite exhibited bands in the range 1300–1700 cm^{-1} which were not detected in the latter. The reasons for the occurrence of a different hydrolysis process are, however, not clear. Since the two parent ZSM-5 zeolites differed mainly in the Si/Al ratio, textural properties (Table 1), crystallites size, and the presence of extraframework Al species (Fe/ZSM-5(15)), a relationship between their physicochemical properties and the nature of the Fe species is expected. Particularly, the presence of extraframework Al species, usually ascribed to (hydr)oxo moieties, might favor the formation of the iron oxide. Since Fe and Al oxide compounds have similar structural properties, it can be envisaged that the presence of extraframework Al species might induce the epitaxial growth of the Fe oxides, thus hindering the rearrangement of Fe into binuclear species. Further investigations are in progress in order to determine the species formed on Fe/ZSM-5(20) after hydrolysis, which might provide a more precise understanding of the structure of the active species on this catalyst.

CONCLUSIONS

The state of iron in two Fe/ZSM-5 zeolites prepared by sublimation of $FeCl_3$ was investigated by means of XRD, IR, ^{27}Al MAS NMR, EXAFS, and nitrogen adsorption measurements. EXAFS results clearly indicated that Fe is hosted on the two zeolites in different forms. In one case (Fe/ZSM-5(20)), Fe was found in the form of diferric binuclear clusters featuring a diamond core similar to that of the monooxygenase enzyme. On the basis of the IR and NMR results, these complexes were concluded to compensate either one or two negative charges of the lattice, while the remaining ion sites are occupied by Brønsted hydroxyls. In the second case (Fe/ZSM-5(15)), the postexchange treatments converted the iron mainly into hematite particles although a minor fraction of binuclear oxo-bridged species might be present as well. IR spectroscopy suggested that the differences observed in the state of the iron are related to different hydrolysis processes occurring on the two zeolites. The extraframework Al species inside the zeolite pores might play a role in the formation of the iron oxide by favouring its epitaxial growth on the Al species.

ACKNOWLEDGMENTS

The authors thank the Swiss-Norwegian Beamline staff for assistance during the EXAFS measurements at ESRF and Süd Chemie and Zeolyst for kindly providing the zeolites used in this study. We also thank Dr. M. Haouas for carrying out the NMR measurements. This work was supported by the Swiss National Foundation and R'EQUIP grant 2160-053285.98/1.

REFERENCES

1. Morice, J. A., and Rees, L. V. C., *Trans. Faraday Soc.* **64**, 1388 (1968).
2. Garten, L. R., Delgass, W. N., and Boudart, M., *J. Catal.* **18**, 90 (1970).
3. Ermolenko, N. F., Tsybul'skaya, Y. V., and Malashevich, L. N., *Kinet. Catal.* **14**, 904 (1973).
4. Feng, X., and Hall, W. K., *J. Catal.* **166**, 368 (1997).
5. Chen, H.-Y., and Sachtler, W. M. H., *Catal. Today* **42**, 73 (1998).
6. Hall, W. K., Feng, X., Dumesic, J., and Watwe, R., *Catal. Lett.* **52**, 13 (1998).
7. Kucherov, A. V., Montreuil, C. N., Kucherova, T. N., and Shelef, M., *Catal. Lett.* **56**, 173 (1998).
8. Marturano, P., Kogelbauer, A., and Prins, R., *Stud. Surf. Sci. Catal.* **125**, 619 (1999).
9. Kögel, M., Mönnig, R., Schwieger, W., Tissler, A., and Turek, T., *J. Catal.* **182**, 470 (1999).
10. Joyner, R., and Stockenhuber, M., *J. Phys. Chem. B* **103**, 5963 (1999).
11. Long, R. Q., and Yang, R. T., *J. Am. Chem. Soc.* **121**, 5595 (1999).
12. Voskoboinikov, T. V., Chen, H.-Y., and Sachtler, W. M. H., *Appl. Catal. B* **19**, 279 (1998).
13. El-Malki, E.-M., van Santen, R. A., and Sachtler, W. M. H., *J. Phys. Chem. B* **103**, 4611 (1999).
14. Ma, A.-Z., and Grünert, W., *Chem. Commun.* 71 (1999).
15. Lobree, L. J., Hwang, I.-C., Reimer, J. A., and Bell, A. T., *J. Catal.* **186**, 242 (1999).
16. van Zon, J. B. A. D., Koningsberger, D. C., van't Blik, H. F. J., and Sayers, D. E., *J. Chem. Phys.* **82**, 5742 (1985).
17. Kirlin, P. S., van Zon, F. B. M., Koningsberger, D. C., and Gates, B. C., *J. Phys. Chem.* **94**, 8439 (1990).
18. Zabinsky, S. I., Rehr, J. J., Ankudinov, A., Albers, R. C., and Eller, M. J., *Phys. Rev. B* **52**, 2995 (1995).
19. Shirane, G., Pickart, S. J., Nathans, R., and Ishikawa, Y., *J. Phys. Chem. Solids* **10**, 35 (1959).
20. Smyth, J. R., *Am. Mineral.* **60**, 1092 (1975).
21. Ravel, B., ATOMS, Version 2.44 b, The University of Washington, 1995.

22. Zecchina, A., Bordiga, S., Spoto, G., Scarano, D., Petrini, G., Leofanti, G., Padovan, M., and Otero Areàn, C., *J. Chem. Soc., Faraday Trans.* **88**, 2959 (1992).
23. Knözinger, H., *in* "Elementary Reaction Steps in Heterogeneous Catalysis" (R. W. Joyner and R. A. van Santen, Eds.), Vol. 398, p. 267. Kluwer Academic Publisher, Dordrecht, 1993.
24. Lee, H.-T., and Rhee, H.-K., *Catal. Lett.* **61**, 71 (1999).
25. Cornell, R. M., and Schwertmann, U., "The Iron Oxides: Structure, Properties, reactions, Occurrence and Uses." VCH, Weinheim, 1996.
26. "Sadtler Spectra Collection Index." BIO-RAD Sadtler Research Laboratories Ltd., Hemel Hempstead, Herts, U.K., 1994.
27. Webb, G. A., *in* "Nuclear Magnetic Resonance Spectroscopy of Nuclei other than Protons" (T. Axenrod and G. A. Webb, Eds.). Wiley, New York, 1974.
28. Sohár, P., "Nuclear Magnetic Resonance Spectroscopy." CRC Press, Inc., Boca Raton, FL, 1983.
29. Kulshreshtha, S. H., Vijayalakshmi, R., and Sudarsan, V., *Stud. Surf. Sci. Catal.* **113**, 699 (1998).
30. Vieira, A., Tovar, M. A., Pfaff, C., Betancourt, A., Méndez, B., Lopez, C. M., Machado, F. J., Goldwasser, J., Ramirez de Agudelo, M. M., and Houalla, M., *J. Mol. Catal. A* **144**, 101 (1999).
31. Engelhardt, G., Feuerstein, M., Sieger, P., Markgraber, D., Stucky, G., and Srdanov, V., *Chem. Commun.* 729 (1996).
32. Engelhardt, G., *in* "Solid-State NMR Spectroscopy of Inorganic Materials" (J. J. Fitzgerald, Ed.), Vol. 717, p. 266. Am. Chem. Soc., Washington, DC, 1999.
33. Yang, C., and Xu, Q., *Zeolites* **19**, 404 (1997).
34. Axon, S. A., Fox, K. K., Carr, S. W., and Klinowski, J., *Chem. Phys. Lett.* **189**, 1 (1992).
35. Lewis, D. W., Sankar, G., Catlow, C. R. A., Carr, S. W., and Thomas, J. M., *Nucl. Instrum. Methods Phys. Res. B* **97**, 44 (1995).
36. Rey, F., Sankar, G., Maschmeyer, T., Thomas, J. M., Bell, R. G., and Greaves, G. N., *Top. Catal.* **3**, 21 (1996).
37. Bordiga, S., Buzzoni, R., Geobaldo, F., Lamberti, C., Giamello, E., Zecchina, A., Leofanti, G., Petrini, G., Tozzola, G., and Vlaic, G., *J. Catal.* **158**, 486 (1996).
38. Patarin, J., Tulier, M. H., Durr, J., and Kessler, H., *Zeolites* **12**, 70 (1992).
39. Lewis, D. W., Catlow, C. R. A., Sankar, G., and Carr, S. W., *J. Phys. Chem.* **99**, 2377 (1995).
40. Kissinger, C. R., Adman, E. T., Sicker, C. C., and Jensen, L. H., *J. Am. Chem. Soc.* **110**, 8721 (1988).
41. Cramer, S. P., *in* "X-ray Absorption, Principles, Applications, Techniques of EXAFS, SEXAFS and XANES" (D. C. Koningsberger and R. Prins, Eds.). Wiley, New York, 1988.
42. Yoo, S. J., Hu, Z., Goh, C., Bominaar, E. L., Holm, R. H., and Münck, E., *J. Am. Chem. Soc.* **119**, 8732 (1997).
43. Goh, C., Nivorozhkin, A., Yoo, S. J., Bominaar, E. L., Münck, E., and Holm, R. H., *Inorg. Chem.* **37**, 2923 (1998).
44. Dubkov, K. A., Sobolev, V. I., Talsi, E. P., Rodkin, M. A., Watkins, N. H., Shteinman, A. A., and Panov, G. I., *J. Mol. Catal. A* **123**, 155 (1997).
45. Panov, G. I., Uriarte, A. K., Rodkin, M. A., and Sobolev, V. I., *Catal. Today* **41**, 365 (1998).
46. Wallar, B. J., and Lipscomb, J. D., *Chem. Rev.* **96**, 2625 (1996).
47. Prince, R. C., George, G. N., Savas, J. C., Cramer, S. P., and Patel, R. N., *Biochim. Biophys. Acta* **952**, 220 (1988).
48. Shu, L., Liu, Y., Lipscomb, J. D., and Que, L. J., *J. Biol. Inorg. Chem.* **1**, 297 (1996).
49. Rosenzweig, A. C., Nordlund, P., Takahara, P. M., Frederick, C. A., and Lippard, S. J., *Chem. Biol.* **2**, 409 (1995).
50. Zhang, Y., Dong, Y., Que, L. J., Kauffmann, K., and Münck, E., *J. Am. Chem. Soc.* **117**, 1169 (1995).
51. Zheng, H., Zhang, Y., Dong, Y., Young, V. G., and Que, L. J., *J. Am. Chem. Soc.* **121**, 2226 (1999).
52. Zhang, Y., Pan, G., Que, L. J., Fox, B. G., and Münck, E., *J. Am. Chem. Soc.* **116**, 3653 (1994).
53. Ou, C. C., Lalancette, R. A., Potenza, J. A., and Schugar, H. J., *J. Am. Chem. Soc.* **100**, 2053 (1978).
54. Thich, J. A., Ou, C. C., Powers, D., Vasilion, B., Mastropaolo, D., Potenza, J. A., and Schugar, H. J., *J. Am. Chem. Soc.* **98**, 1425 (1976).
55. Borer, L., Thalken, L., Ceccarelli, C., Glick, M., Zhang, J. H., and Reiff, W. M., *Inorg. Chem.* **22**, 1719 (1983).
56. Rosenzweig, A. C., Frederick, C. A., Lippard, S. J., and Nordlund, P., *Nature* **366**, 537 (1993).
57. Hwang, J., Krebs, C., Hanh Huynh, B., Edmondson, D. E., Theil, E. C., and Penner-Hanh, J. E., *Science* **287**, 122 (2000).
58. Goodman, B. R., Hass, K. C., Schneider, W. F., and Adams, J. B., *J. Phys. Chem. B* **103**, 10452 (1999).